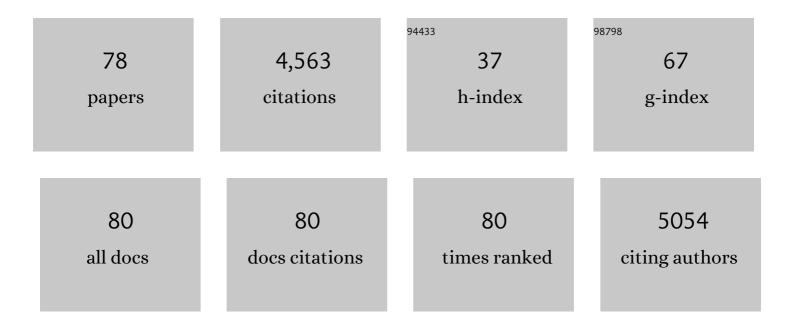
List of Publications by Year in descending order

Source: https://exaly.com/author-pdf/6590857/publications.pdf Version: 2024-02-01



Μλάκ Μιιτι

#	Article	IF	CITATIONS
1	Hypoxia and Glucose Metabolism in Malignant Tumors. Clinical Cancer Research, 2004, 10, 2245-2252.	7.0	375
2	Regional Hypoxia in Glioblastoma Multiforme Quantified with [18F]Fluoromisonidazole Positron Emission Tomography before Radiotherapy: Correlation with Time to Progression and Survival. Clinical Cancer Research, 2008, 14, 2623-2630.	7.0	257
3	Imaging P-glycoprotein transport activity at the human blood-brain barrier with positron emission tomography. Clinical Pharmacology and Therapeutics, 2005, 77, 503-514.	4.7	243
4	In vivo validation of 3'deoxy-3'-[(18)F]fluorothymidine ([(18)F]FLT) as a proliferation imaging tracer in humans: correlation of [(18)F]FLT uptake by positron emission tomography with Ki-67 immunohistochemistry and flow cytometry in human lung tumors. Clinical Cancer Research, 2002, 8, 3315-23.	7.0	236
5	Tumor-Specific Positron Emission Tomography Imaging in Patients: [18F] Fluorodeoxyglucose and Beyond. Clinical Cancer Research, 2007, 13, 3460-3469.	7.0	154
6	Multimodality Brain Tumor Imaging: MR Imaging, PET, and PET/MR Imaging. Journal of Nuclear Medicine, 2015, 56, 1554-1561.	5.0	152
7	Quantitative Metrics of Net Proliferation and Invasion Link Biological Aggressiveness Assessed by MRI with Hypoxia Assessed by FMISO-PET in Newly Diagnosed Glioblastomas. Cancer Research, 2009, 69, 4502-4509.	0.9	147
8	Complementary but Distinct Roles for MRI and <sup>18</sup> F-Fluoromisonidazole PET in the Assessment of Human Glioblastomas. Journal of Nuclear Medicine, 2009, 50, 36-44.	5.0	137
9	18F-FDG PET of gliomas at delayed intervals: improved distinction between tumor and normal gray matter. Journal of Nuclear Medicine, 2004, 45, 1653-9.	5.0	130
10	Imaging of Cyclosporine Inhibition of P-Glycoprotein Activity Using <sup>11</sup> C-Verapamil in the Brain: Studies of Healthy Humans. Journal of Nuclear Medicine, 2009, 50, 1267-1275.	5.0	127
11	Variations of Dynamic Contrast-Enhanced Magnetic Resonance Imaging in Evaluation of Breast Cancer Therapy Response: A Multicenter Data Analysis Challenge. Translational Oncology, 2014, 7, 153-166.	3.7	120
12	Kinetic analysis of 3'-deoxy-3'-fluorothymidine PET studies: validation studies in patients with lung cancer. Journal of Nuclear Medicine, 2005, 46, 274-82.	5.0	108
13	Metabolism of 3′-deoxy-3′-[F-18]fluorothymidine in proliferating A549 cells: Validations for positron emission tomography. Nuclear Medicine and Biology, 2004, 31, 829-837.	0.6	102
14	Kinetic analysis of 3'-deoxy-3'-18F-fluorothymidine in patients with gliomas. Journal of Nuclear Medicine, 2006, 47, 1612-21.	5.0	102
15	ACRIN 6684: Assessment of Tumor Hypoxia in Newly Diagnosed Glioblastoma Using 18F-FMISO PET and MRI. Clinical Cancer Research, 2016, 22, 5079-5086.	7.0	99
16	PET Tumor Metabolism in Locally Advanced Breast Cancer Patients Undergoing Neoadjuvant Chemotherapy: Value of Static versus Kinetic Measures of Fluorodeoxyglucose Uptake. Clinical Cancer Research, 2011, 17, 2400-2409.	7.0	94
17	18F-FDG kinetics in locally advanced breast cancer: correlation with tumor blood flow and changes in response to neoadjuvant chemotherapy. Journal of Nuclear Medicine, 2004, 45, 1829-37.	5.0	92
18	Verapamil P-glycoprotein Transport across the Rat Blood-Brain Barrier: Cyclosporine, a Concentration Inhibition Analysis, and Comparison with Human Data. Journal of Pharmacology and Experimental Therapeutics, 2006, 317, 704-710.	2.5	87

#	Article	IF	CITATIONS
19	True tracers: comparing FDG with glucose and FLT with thymidine. Nuclear Medicine and Biology, 2005, 32, 663-671.	0.6	85
20	Quantitative assessment of dynamic PET imaging data in cancer imaging. Magnetic Resonance Imaging, 2012, 30, 1203-1215.	1.8	84
21	Kinetic modeling of 3'-deoxy-3'-fluorothymidine in somatic tumors: mathematical studies. Journal of Nuclear Medicine, 2005, 46, 371-80.	5.0	80
22	C11-Acetate and F-18 FDG PET for Men With Prostate Cancer Bone Metastases. Clinical Nuclear Medicine, 2011, 36, 192-198.	1.3	76
23	A Phase II Study of 3′-Deoxy-3′- <sup>18</sup> F-Fluorothymidine PET in the Assessment of Early Response of Breast Cancer to Neoadjuvant Chemotherapy: Results from ACRIN 6688. Journal of Nuclear Medicine, 2015, 56, 1681-1689.	5.0	73
24	The Impact of Arterial Input Function Determination Variations on Prostate Dynamic Contrast-Enhanced Magnetic Resonance Imaging Pharmacokinetic Modeling: A Multicenter Data Analysis Challenge. Tomography, 2016, 2, 56-66.	1.8	70
25	The FDG lumped constant in normal human brain. Journal of Nuclear Medicine, 2002, 43, 1157-66.	5.0	70
26	Kinetic Analysis of <sup>18</sup> F-Fluoride PET Images of Breast Cancer Bone Metastases. Journal of Nuclear Medicine, 2010, 51, 521-527.	5.0	65
27	Comparison of different quantitative approaches to 18F-fluoride PET scans. Journal of Nuclear Medicine, 2004, 45, 1493-500.	5.0	64
28	Dynamic and Static Approaches to Quantifying 18F-FDG Uptake for Measuring Cancer Response to Therapy, Including the Effect of Granulocyte CSF. Journal of Nuclear Medicine, 2007, 48, 920-925.	5.0	61
29	Castration-Resistant Prostate Cancer Bone Metastasis Response Measured by <sup>18</sup> F-Fluoride PET After Treatment with Dasatinib and Correlation with Progression-Free Survival: Results from American College of Radiology Imaging Network 6687. Journal of Nuclear Medicine, 2015, 56, 354-360.	5.0	55
30	Errors in Quantitative Image Analysis due to Platform-Dependent Image Scaling. Translational Oncology, 2014, 7, 65-71.	3.7	51
31	Positron Emission Tomography Imaging of [ <sup>11</sup> C]Rosuvastatin Hepatic Concentrations and Hepatobiliary Transport in Humans in the Absence and Presence of Cyclosporin A. Clinical Pharmacology and Therapeutics, 2019, 106, 1056-1066.	4.7	51
32	18F-Fluorothymidine radiation dosimetry in human PET imaging studies. Journal of Nuclear Medicine, 2003, 44, 1482-8.	5.0	51
33	Kinetic characterization of hexokinase isoenzymes from glioma cells: Implications for FDG imaging of human brain tumors. Nuclear Medicine and Biology, 2001, 28, 107-116.	0.6	50
34	2-[(18)F]Fluoro-2-deoxyglucose and glucose uptake in malignant gliomas before and after radiotherapy: correlation with outcome. Clinical Cancer Research, 2002, 8, 971-9.	7.0	49
35	Simultaneous PET Imaging of P-Glycoprotein Inhibition in Multiple Tissues in the Pregnant Nonhuman Primate. Journal of Nuclear Medicine, 2009, 50, 798-806.	5.0	47
36	The Impact of Arterial Input Function Determination Variations on Prostate Dynamic Contrast-Enhanced Magnetic Resonance Imaging Pharmacokinetic Modeling: A Multicenter Data Analysis Challenge, Part II. Tomography, 2019, 5, 99-109.	1.8	44

#	Article	IF	CITATIONS
37	Multisite Concordance of DSC-MRI Analysis for Brain Tumors: Results of a National Cancer Institute Quantitative Imaging Network Collaborative Project. American Journal of Neuroradiology, 2018, 39, 1008-1016.	2.4	43
38	Applying a patient-specific bio-mathematical model of glioma growth to develop virtual [18F]-FMISO-PET images. Mathematical Medicine and Biology, 2012, 29, 31-48.	1.2	41
39	Prospective Study of Serial <sup>18</sup> F-FDG PET and <sup>18</sup> F-Fluoride PET to Predict Time to Skeletal-Related Events, Time to Progression, and Survival in Patients with Bone-Dominant Metastatic Breast Cancer. Journal of Nuclear Medicine, 2018, 59, 1823-1830.	5.0	41
40	Determination of the Deoxyglucose and Glucose Phosphorylation Ratio and the Lumped Constant in Rat Brain and a Transplantable Rat Glioma. Journal of Neurochemistry, 1989, 53, 37-44.	3.9	35
41	18F-Fluoromisonidazole Quantification of Hypoxia in Human Cancer Patients Using Image-Derived Blood Surrogate Tissue Reference Regions. Journal of Nuclear Medicine, 2015, 56, 1223-1228.	5.0	33
42	What is in a number? The FDG lumped constant in the rat brain. Journal of Nuclear Medicine, 2007, 48, 5-7.	5.0	32
43	Modeling Cyclosporine A Inhibition of the Distribution of a P-Glycoprotein PET Ligand, <sup>11</sup> C-Verapamil, into the Maternal Brain and Fetal Liver of the Pregnant Nonhuman Primate: Impact of Tissue Blood Flow and Site of Inhibition. Journal of Nuclear Medicine, 2013, 54, 437-446.	5.0	29
44	Deoxyglucose Kinetics in a Rat Brain Tumor. Journal of Cerebral Blood Flow and Metabolism, 1989, 9, 315-322.	4.3	27
45	Multiagent PET for Risk Characterization in Sarcoma. Journal of Nuclear Medicine, 2011, 52, 541-546.	5.0	27
46	Nonparametric Residue Analysis of Dynamic PET Data With Application to Cerebral FDG Studies in Normals. Journal of the American Statistical Association, 2009, 104, 556-571.	3.1	25
47	Evaluating Multisite rCBV Consistency from DSC-MRI Imaging Protocols and Postprocessing Software Across the NCI Quantitative Imaging Network Sites Using a Digital Reference Object (DRO). Tomography, 2019, 5, 110-117.	1.8	25
48	Multiâ€ <b>s</b> ite quality and variability analysis of 3D FDG PET segmentations based on phantom and clinical image data. Medical Physics, 2017, 44, 479-496.	3.0	22
49	Multisite concordance of apparent diffusion coefficient measurements across the NCI Quantitative Imaging Network. Journal of Medical Imaging, 2017, 5, 1.	1.5	22
50	Multicenter Clinical Trials Using 18F-FDG PET to Measure Early Response to Oncologic Therapy: Effects of Injection-to-Acquisition Time Variability on Required Sample Size. Journal of Nuclear Medicine, 2016, 57, 226-230.	5.0	21
51	ACRIN 6684: Multicenter, phase II assessment of tumor hypoxia in newly diagnosed glioblastoma using magnetic resonance spectroscopy. PLoS ONE, 2018, 13, e0198548.	2.5	21
52	Test–Retest Reproducibility of <sup>18</sup> F-FDG PET/CT Uptake in Cancer Patients Within a Qualified and Calibrated Local Network. Journal of Nuclear Medicine, 2019, 60, 608-614.	5.0	21
53	Deoxyglucose Lumped Constant Estimated in a Transplanted Rat Astrocytic Glioma by the Hexose Utilization Index. Journal of Cerebral Blood Flow and Metabolism, 1990, 10, 190-198.	4.3	18
54	Assessment of the Prognostic Value of Radiomic Features in 18F-FMISO PET Imaging of Hypoxia in Postsurgery Brain Cancer Patients: Secondary Analysis of Imaging Data from a Single-Center Study and the Multicenter ACRIN 6684 Trial. Tomography, 2020, 6, 14-22.	1.8	17

#	Article	IF	CITATIONS
55	Voxel-level mapping of tracer kinetics in PET studies: A statistical approach emphasizing tissue life tables. Annals of Applied Statistics, 2014, 8, 1065-1094.	1.1	16
56	Rapid solid-phase extraction method to quantify [11C]-verapamil, and its [11C]-metabolites, in human and macaque plasma. Nuclear Medicine and Biology, 2008, 35, 911-917.	0.6	15
57	Assessment of tumor hypoxia and perfusion in recurrent glioblastoma following bevacizumab failure using MRI and 18F-FMISO PET. Scientific Reports, 2021, 11, 7632.	3.3	15
58	Challenges in clinical studies with multiple imaging probes. Nuclear Medicine and Biology, 2007, 34, 879-885.	0.6	14
59	Quantifying Bias and Precision of Kinetic Parameter Estimation on the PennPET Explorer, a Long Axial Field-of-View Scanner. IEEE Transactions on Radiation and Plasma Medical Sciences, 2020, 4, 735-749.	3.7	13
60	Principles of Tracer Kinetic Analysis in Oncology, Part I: Principles and Overview of Methodology. Journal of Nuclear Medicine, 2022, 63, 342-352.	5.0	13
61	Effect of 18F-FDG Uptake Time on Lesion Detectability in PET Imaging of Early-Stage Breast Cancer. Tomography, 2015, 1, 53-60.	1.8	12
62	18F-fluorodeoxyglucose (FDG) PET or 18F-fluorothymidine (FLT) PET to assess early response to aromatase inhibitors (AI) in women with ER+ operable breast cancer in a window-of-opportunity study. Breast Cancer Research, 2021, 23, 88.	5.0	11
63	Multiâ€Site Concordance of Diffusionâ€Weighted Imaging Quantification for Assessing Prostate Cancer Aggressiveness. Journal of Magnetic Resonance Imaging, 2022, 55, 1745-1758.	3.4	11
64	Blood flow in an experimental rat brain tumor by tissue equilibration and indicator fractionation. Journal of Neuro-Oncology, 1987, 5, 37-46.	2.9	9
65	Chronic elevation of plasma vascular endothelial growth factor-A (VEGF-A) is associated with a history of blast exposure. Journal of the Neurological Sciences, 2020, 417, 117049.	0.6	9
66	Imaging Hypoxia with 18F-Fluoromisonidazole: Challenges in Moving to a More Complicated Analysis. Journal of Nuclear Medicine, 2016, 57, 497-498.	5.0	6
67	Functional 4-D clustering for characterizing intratumor heterogeneity in dynamic imaging: evaluation in FDG PET as a prognostic biomarker for breast cancer. European Journal of Nuclear Medicine and Molecular Imaging, 2021, 48, 3990-4001.	6.4	6
68	Assessment of a statistical AIF extraction method for dynamic PET studies with 15O water and 18F fluorodeoxyglucose in locally advanced breast cancer patients. Journal of Medical Imaging, 2017, 5, 1.	1.5	6
69	Principles of Tracer Kinetic Analysis in Oncology, Part II: Examples and Future Directions. Journal of Nuclear Medicine, 2022, 63, 514-521.	5.0	5
70	Whole-Body [18F]-Fluoride PET SUV Imaging to Monitor Response to Dasatinib Therapy in Castration-Resistant Prostate Cancer Bone Metastases: Secondary Results from ACRIN 6687. Tomography, 2021, 7, 139-152.	1.8	4
71	Quantitation of multiple injection dynamic PET scans: an investigation of the benefits of pooling data from separate scans when mapping kinetics. Physics in Medicine and Biology, 2021, 66, 135010.	3.0	4
72	Inter-operator variability in compartmental kinetic analysis of 18 F-fluoromisonidazole dynamic PET. Clinical Imaging, 2018, 49, 121-127.	1.5	2

#	Article	IF	CITATIONS
73	An Illustration of the Use of Model-Based Bootstrapping for Evaluation of Uncertainty in Kinetic Information Derived from Dynamic PET. , 2019, , .		2
74	A digital reference object for the 3D Hoffman brain phantom for characterization of PET neuroimaging quality. , 2013, , .		1
75	Kinetic analysis of dynamic <sup>18</sup> F-FDG and <sup>15</sup> O-H <inf>2</inf> O PET studies by parametric and nonparametric methods: A statistical analysis. , 2011, , .		0
76	Improving lesion detectability in low uptake 18 F-FDG breast cancer by optimizing PET imaging time. , 2014, , .		0
77	A Simple Evaluation of the Benefit of Combined Kinetic Analysis of Multiple Injection Dynamic PET Scans. , 2019, , .		0
78	An exploration of the prognostic utility of shortened dynamic imaging protocols for PET-FDG scans. , 2019, , .		0